

Millimeter Wave Receiver Efficiency: A Comprehensive Comparison of Beamforming Schemes with Low Resolution ADCs

Waqas bin Abbas, Felipe Gomez-Cuba, Michele Zorzi *Fellow, IEEE*

Abstract

In this work, we study the achievable rate and the energy efficiency of Analog, Hybrid and Digital Combining (AC, HC and DC) for millimeter wave (mmW) receivers. We take into account the power consumption of all receiver components, not just Analog-to-Digital Converters (ADC), determine some practical limitations of beamforming in each architecture, and develop performance analysis charts that enable comparison of different receivers simultaneously in terms of two metrics, namely, Spectral Efficiency (SE) and Energy Efficiency (EE). We present a multi-objective utility optimization interpretation to find the best SE-EE weighted trade-off among AC, DC and HC schemes. We consider an Additive Quantization Noise Model (AQNM) to evaluate the achievable rates with low resolution ADCs. Our analysis shows that AC is only advantageous if the channel rank is strictly one, the link has very low SNR, or there is a very stringent low power constraint at the receiver. Otherwise, we show that the usual claim that DC requires the highest power is not universally valid. Rather, either DC or HC alternatively result in the better SE vs EE trade-off depending strongly on the considered power consumption characteristic values for each component of the mmW receiver.

Index Terms

Millimeter Wave, Analog Beamforming, Hybrid Beamforming, Digital Beamforming, Energy Efficiency, Spectral Efficiency, Low Resolution ADCs

Part of this work was presented at the European Wireless 2016 and 2017 conferences, Oulu, Finland and Dresden, Germany, respectively, [1], [2]. Waqas Bin Abbas was with the Department of Information Engineering, University of Padova, Italy and is now with National University of Computer and Emerging Sciences, Islamabad, Pakistan. waqas.abbas@nu.edu.pk. Michele Zorzi is with the Department of Information Engineering, University of Padova, Italy. zorzi@dei.unipd.it. Felipe Gomez-Cuba was with the University of Vigo, Spain, and is now with the University of Padova, Italy. fgomez@gti.uvigo.es. Work supported by FPU12/01319.

I. INTRODUCTION

The millimeter wave (mmW) spectrum (10-300 GHz)¹, where a very large bandwidth is available, is considered as a prime candidate to fulfill the data rate requirements of future broadband communication [3]–[7]. However, communication in these frequency bands exhibits high pathloss [3]. To overcome this problem, spatial beamforming/combining using large antenna arrays is considered as an essential part of a mmW communication system.

Analog, Hybrid and Digital beamforming/combining schemes are being considered for mmW MIMO communication systems [8]. Although a fully digital architecture, which requires a separate RF chain per antenna element, is a popular choice in classical systems, it is not generally considered as a viable option for large antenna arrays due to the high power consumption assumed for analog-digital signal processing components [9]. This is even more critical at mmW frequencies, as the power consumption of an Analog to Digital Converter (ADC) in a receiver grows linearly with the system bandwidth. However, multiple options exist to reduce the power consumption, i.e.:

- 1) The use of Analog Combining (AC), which requires a single Radio-Frequency (RF) plus ADC chain. AC consumes the least power and is an attractive choice whenever the advantages of digital processing techniques (mainly spatial multiplexing) are not required [10].
- 2) The use of Hybrid Combining (HC), which performs combining in both the analog and the digital domain with a reduced number of RF chains, at the cost of lower flexibility than fully digital architectures [11].
- 3) The use of low-resolution ADCs (for example, 1-4 bits) while maintaining the Digital Combining (DC) MIMO architecture [12], [13].

Our recent work [1] showed that unlike usually claimed, DC does not always have worse power efficiency than HC, if we take into account the power consumption of all analog receiver components necessary for both DC and HC. Rather, there are regimes (specifically with a small number of ADC bits and at lower bandwidth) where DC can still result in a lower power consumption than HC.

¹Although a rigorous definition of mmW frequencies would place them between 30 and 300 GHz, industry has loosely defined them to include the spectrum from 10 to 300 GHz.

In this paper, we extend our analysis and provide a comprehensive characterization of the Spectral Efficiency (SE, defined as rate/bandwidth) versus the Energy Efficiency (EE, defined as rate/total power consumption) of AC, HC and DC architectures for a wide variety of possible scenarios. We argue that the popular claim that DC always has the highest power consumption is limited to models based solely on ADC power with many bits. Rather, the choice between DC and HC critically depends on the specific technical characteristics of analog receiver components, and even environmental changes (such as a transition from LOS to NLOS decreasing SNR by -20dB) may significantly affect the SE vs EE trade-off. Using values for low-power ADC technologies and moderately high-power Phase Shifter (PS) components, low-resolution DC is preferable, whereas receivers fabricated with (presumably cheaper) high-power ADCs and lower-power PS instead demand the use of HC designs. We highlight that the conclusions in the literature regarding energy efficient receiver design are primarily based on specific examples of typical receiver components/parameters (e.g., the ADC Walden's figure of merit). Therefore many such conclusions are applicable to the component parameters chosen as a reference, but may not be easily extrapolated into a general case. Instead, in this paper we show that the choice of the appropriate combining scheme at the receiver directly depends on the selected set of receiver components and parameters, e.g., we will show in Section V that HC can perform better than DC in an Uplink scenario only if the number of RF chains is carefully selected, whereas DC outperforms HC with a poorly chosen number of RF chains. Therefore, the main contribution of this work lies in highlighting this key dependency and in the provided framework for comparison itself, rather than in the specific comparisons that we give as examples for a given set of reference parameters. For this reason we are also providing a web tool [14] where readers can generate charts following our framework but substituting their own component parameters. Our analysis shows that:

- EE is convex in the number of bits and achieves a maximum at a certain optimal resolution that is directly related to the SNR and inversely related to the ADC power figure of merit.
- AC achieves both the best SE and EE when the mmW channel has rank 1 and/or in very low SNR links, and is the only viable architecture under a very stringent power constraint. Due to the fact that mmW propagation experiences high attenuation, most scattered reflections become too attenuated and the mmW channel is dominated by a sparse set of reflectors. Therefore, if we remove all channel contributions that are too small and buried by the noise,

approximate mmW channel rank-1 matrix representations arise with a notable probability. For example, it is noted in [15] that for the median channel a single spatial dimension carries approximately 50% of the propagated energy and two degrees of freedom capture 80% of the channel energy. We also performed a small Monte-Carlo trial with 10^4 channel realizations, and found that the first eigenvalue represents over 50% of the total channel energy with probability 0.95 and over 75% of the energy with probability 0.6. We also observed that the second channel eigenvalue was often one order of magnitude smaller than the first.

- DC always outperforms HC in terms of SE. In some cases it also has better EE, while in other cases DC with 3-5 bits offers a trade-off with some more SE and only slightly worse EE than HC. This depends critically on how pessimistic are the ADC and Phase Shifter power models, the SNR (which is affected by channel pathloss and fading), the number of receiver antennas, and the number of parallel RF lines in the HC architecture. There is no one-size-fits-all universally best scheme.

In summary, when considering the total power consumption of the receiver instead of just focusing on the ADC power consumption, in a non-negligible range of scenarios DC may be preferable over HC. Particularly, DC may be a better choice than HC in a Downlink connection (where the receiver is equipped with a not-so-large number of antennas) whereas HC may be a better option in an Uplink connection. In addition, future mmW system characteristics are not yet completely settled, so DC has the additional advantage of versatility. On the other hand, HC can potentially have additional advantages in terms of component dimensions and cost. Moreover, reducing the number of ADC bits reduces the rate of the fronthaul (the optical communication between the radio head and the baseband processor).

It must also be highlighted that the use of low precision ADCs may make it difficult to accurately estimate the channel [16]–[18]. As a first step, in this paper we have focused on studying the SE vs EE trade-off assuming perfect CSI, while the extension of these results to imperfect CSI and the comparison of other engineering metrics such as cost, dimensions and fronthaul rates are left for future extensions of our work.

A. Related Work

Recent works study energy efficient designs, particularly focusing on how the system rate varies as a function of the ADC resolution. In [19], the rate of a quantized MIMO system with coding has been studied, while in [20] the rate and bit error rate of a quantized MIMO system were analyzed. In [21], a rate lower bound for a quantized MIMO system with Gaussian input was analyzed. However, the quantized rate model provides a good approximation only at low SNR. In [22], an exact nonlinear quantizer model is utilized to evaluate the optimal rate for a 1-bit ADC. In [23], considering a MIMO channel and an additive quantization noise model (AQNM, an approximate model for ADCs), a joint optimization of the ADC resolution and the number of antennas is studied. In a recent work [24], the authors studied how the number of ADC bits b and the bandwidth (sampling rate) B of ADCs affect the total power consumption for AC and DC based receivers with a stringent power constraint, such as a mobile station. They studied the optimal b and B which maximize the rate for AC and DC for low power receiver design while also showing that DC with a similar power budget to AC may achieve a higher rate than AC when channel state information is available at the transmitter. In another recent work [25], the EE and SE for low resolution ADC HC architecture is studied. The authors show the advantages of a low resolution HC with few RF chains over an infinite resolution ADC for DC and HC.

Recently, energy efficient architectures for HC were proposed in [26], [27]. In [26], an energy efficient HC architecture has been proposed where each RF chain is only connected to a subset of antennas. In [27], switch based architectures are proposed, where only a reduced set of antennas (as many as the number of RF chains) is selected and connected to the RF chains. However, both proposed architectures result in a lower SE than the fully connected phase shifter architecture.

In [28], [29], the SE of uplink massive MIMO with low resolution ADCs is studied, and it is shown that few ADC bits are enough to achieve almost the same SE of unquantized MIMO. Also, using a 2-bit ADC achieves good performance for a small Rician k -factor [28].

Note that in recent literature DC is either compared with HC [25] or with AC [24] exclusively in terms of EE, which measures in a single dimension capacity divided by power. Therefore, the trade-off between EE and SE in the receiver is not sufficiently well represented, in the sense that existing works recommend the architecture to maximize EE without taking into account how the choice affects the SE. In this work we focus explicitly on this trade-off while considering all

three architectures (AC, DC and HC), rather than separately comparing only the EE of a pair of MIMO techniques. We would like to highlight that our model complements previous works with respect to several aspects:

- First, some works on HC benchmark their proposal against ideal unquantized DC [11], [27], [30]; thus, rather than evaluating which architecture requires less power, these works focus on how close HC performance is to ideal DC. This framework inherently assumes that HC is preferable over low-resolution DC, whereas we show that this may not be true in certain cases.
- Second, some works do not account for some components in the HC architecture, such as the signal splitters (SP) or phase shifters (PS) [9], [11], which may actually have a non-negligible power signature. Our analysis, instead, takes into account the power consumption of *all* components of the receivers considered in the recent literature [24], [27].
- Third, we take into account that system designers may express different preferences for SE and EE according to the application requirements. We express such preference as a multi-objective utility maximization problem where the relative weight of SE vs EE is a free parameter. This gives new insights on the choice between HC and DC that complements the separate analysis of their EE in [25].
- Fourth, we consider point-to-point Downlink and Uplink scenarios to study the effect of the number of receive antennas. The results show that for the Downlink (i.e., the case of a mobile receiver with fewer antennas), DC always outperforms HC across the SE vs EE tradeoff. On the other hand, in the Uplink case (i.e., a base station receiver with many antennas) DC is preferable if SE and EE have similar importance, whereas HC is preferable if the operator only desires to maximize EE while accepting a degradation in SE.
- Fifth, we observe that the power consumption figure of merit for ADCs varies by 3 orders of magnitude between different references in the literature. Likewise, the power consumption of phase shifters varies by 2 orders of magnitude in references. We discuss the origin of this variation, and evaluate the three receiver architectures with two types of component models: Firstly, we consider existing state-of-the-art devices, and secondly, we study how the results would change with a plausible future projection of technology improvements, based on existing hardware surveys.
- Sixth, we emphasize that the trade-off between EE and SE is critically dependent on the

component characteristics. A study of power consumption based on only one typical set of values, even if these are very well documented in industry feedback as in [25], can only provide partial results. We encourage independent researchers to reproduce our analysis for their own set of component parameters using a web tool we have made available at [14]. In the tool, our proposed analysis can be extended by the user through the specification of any desired power consumption value for each component.

II. SYSTEM MODEL

In 5G mmW cellular systems, a distinction is usually made between the Base Station (BS) and the User Equipment (UE). Typical UEs feature 16 antennas and 1 W of transmit power, while typical BSs can have 64 or more antennas and 5 W of transmit power in small pico-cells, or 50 W in large macro-cells. Moreover, the system bandwidth varies from 500 MHz up to 7 GHz [24].

For our channel model, however, we simply distinguish between transmitter and receiver roles, where each role may be played by either a BS or a UE depending on the appropriate choice of the parameters for transmitted power and number of transmit and receive antennas. We obtain analytical expressions for SE and EE as a direct function of the number of antennas and of the SNR of the link, obtaining results that apply to all mmW devices. Note that we considered hybrid architectures and finite quantization only at the receiver, whereas we assume that the transmitter implements ideal Digital Preprocessing (DP). This assumption is also used in related works, and is the most relevant case for this paper in which we study whether AC, HC or DC performs better, due to the fact that 1) if HC outperforms DC using DP, then the use of Hybrid Preprocessing can only make DC even worse; and 2) if DC outperforms HC with DP then switching to HP+DC or HP+HC to reduce Digital-Analog Converter (DAC) power consumption is never necessary, because the power consumed by the receiver's ADC is of more concern than that of the transmitter's DAC, and therefore if DC is preferable so will be DP.

We consider a point-to-point multiple input multiple output (MIMO) mmW channel where the transmitter is equipped with N_t antennas and the receiver with N_r antennas. The channel has a flat response over a bandwidth B and a delay spread much smaller than the transmission frame duration, so that inter-symbol interference can be disregarded or simply suppressed using

a prefix of negligible duration². Without inter-symbol interference, the received signal can then be expressed as [31]

$$\mathbf{y} = \mathbf{H}\mathbf{x} + \mathbf{n} \quad (1)$$

where \mathbf{x} and \mathbf{y} represent the transmitted and the received symbol vectors at discrete time instants with period $1/B$, respectively, \mathbf{n} is the i.i.d. circularly symmetric complex Gaussian noise vector, $\mathbf{n} \sim \mathcal{CN}(\mathbf{0}, N_o\mathbf{I})$, and \mathbf{H} represents the $N_r \times N_t$ channel matrix that varies following a fast block-fading model that remains constant for a small number of symbols and takes independent identically distributed (i.i.d.) values across blocks; this means that the rate of the system is the *ergodic rate* (average mutual information over the realizations of \mathbf{H}).

The mmW channel matrix is generated from a random geometric model defined in [6], [15], [30]:

$$\mathbf{H} = \sqrt{\frac{N_t N_r}{\rho N_c N_p}} \sum_{k=1}^{N_c} \sum_{\ell=1}^{N_p} g_{k,\ell} \mathbf{a}_r(\phi_k + \Delta\phi_{k,\ell}) \mathbf{a}_t^H(\theta_k + \Delta\theta_{k,\ell}) \quad (2)$$

where the parameters are randomly generated with the distributions described in Table I.

In this model, the macroscopic SNR depends on a path-loss model that increases with distance by different exponents depending on whether or not the link is in a Line of Sight (LOS) state. We model the antenna arrays at both the transmitter and the receiver as uniform linear arrays (ULA) with adjacent antenna spacing of half the wavelength of the transmitted signal ($\lambda/2$). For small scale fading, a moderate number of propagation paths (order of tens) are generated and grouped in a few clusters (average 1.8). Paths in the same clusters have i.i.d. gains but only narrow random differences in the angles of departure and arrival.

In our evaluations, in addition to the measurement-fit number of clusters and paths considered in [15] ($E[N_c] = 1.8$ and $N_p = 20$), we also consider a rank 1 channel with $N_c = N_p = 1$ to illustrate the effect of the low rank channel matrix \mathbf{H} on the choice of an appropriate combining scheme.

²The assumption of a frequency flat channel is common practice in many mmW receiver analyses in the literature [10], [12], [30]. This is motivated by the fact that due to the high directivity and attenuation, the dominant propagation paths in mmW traverse similar distances and have similar delays, reducing frequency selectivity of the channel. Moreover, all these frequency-flat results are easily extended to frequency-selective models considering orthogonal frequency division multiplexing (OFDM). Extension to single carrier models is also possible.

TABLE I
MMW CHANNEL PROBABILITY DISTRIBUTION [15]

Macroscopic Pathloss in dB (Line of Sight at distance d)	ρ_{LOS} ξ	$61.5 + 20 \log(d) + \xi$ $\sim \mathcal{N}(0, 5.8)$
Macroscopic Pathloss in dB (Non-LOS at distance d)	ρ_{NLOS} ξ	$72 + 29.2 \log(d) + \xi$ $\sim \mathcal{N}(0, 8.7)$
Number of Scattering Clusters	N_c	$\sim \text{Poisson}(1.8)$
Clust. Central Angle of Arrival	ϕ_k	$\sim \text{U}[0, 2\pi]$
Clust. Ctrl. Ang. of Departure	θ_k	$\sim \text{U}[0, 2\pi]$
Number. of Paths per Cluster	N_p	20
Small scale scattering per path	$g_{k,\ell}$	$\mathcal{CN}(0, 1)$
Path Differential AoA	$\Delta\phi_{k,\ell}$	$\sim \mathcal{N}(0, 10^\circ)$
Path Differential AoD	$\Delta\theta_{k,\ell}$	$\sim \mathcal{N}(0, 10^\circ)$
Linear N -antenna Array	$\mathbf{a}(\theta)$	$\begin{pmatrix} 1 \\ e^{j \sin(\theta) \frac{1}{N}} \\ \vdots \\ e^{j \sin(\theta) \frac{N-1}{N}} \end{pmatrix}$

A. Quantized Received signal

The rate of the quantized MIMO channel with a 1 bit ADC under an exact non linear quantization model is shown in [22]. However, such exact non-linear models are difficult to analyze for a higher number of bits. A common lower bound for the achievable rate in quantized systems is obtained modeling the quantization as additive Gaussian noise with power inversely proportional to the resolution of the quantizer, that is, 2^{-b} times the receiver input power where b is the number of ADC bits. In recent studies [24], [28], this Additive Quantization Noise Model (AQNM) has been applied to the study of quantized mmW signals with an arbitrary number of ADC bits. Some other studies [18], [32] have obtained Gaussian approximations for quantization additive distortion following the Bussgang theorem, which in our scenario is very similar to the AQNM.

B. Received Signal Model with AQNM

We consider that the received signals at each antenna may be subject to some analog processing prior to quantization. This RF-processed received signal is converted to the digital domain

TABLE II
 η FOR DIFFERENT VALUES OF b [28]

b	1	2	3	4	5
η	0.3634	0.1175	0.03454	0.009497	0.002499

by multiple ADCs (one ADC for each inphase and quadrature component for each vector dimension). The AQNM represents the quantized version \mathbf{y}_q of the received signal (1) as

$$\mathbf{y}_q = (1 - \eta)(\mathbf{H}\mathbf{x} + \mathbf{n}) + \mathbf{n}_q \quad (3)$$

where \mathbf{n}_q is the additive quantization noise and η is the inverse of the signal-to-quantization noise ratio, which is inversely proportional to the square of the resolution of an ADC (i.e., $\eta \propto 2^{-2b}$). For a Gaussian input distribution, the values of η for $b \leq 5$ are listed in Table II, and for $b > 3$ can be approximated by $\eta = \frac{\pi\sqrt{3}}{2}2^{-2b}$ [28]. We denote by γ_q the signal-to-noise ratio SNR of \mathbf{y}_q , given by

$$\gamma_q = (1 - \eta)^2(\mathbf{H}\mathbf{R}_{\mathbf{xx}}\mathbf{H}^H)((1 - \eta)^2 N_o \mathbf{I} + \mathbf{R}_{\mathbf{n}_q \mathbf{n}_q})^{-1} \quad (4)$$

where superscript H denotes conjugate transpose, $\mathbf{H}\mathbf{R}_{\mathbf{xx}}\mathbf{H}^H$ is the received signal at the output of the quantizer, $\mathbf{R}_{\mathbf{xx}}$ is the input covariance, N_o is the noise power, and $\mathbf{R}_{\mathbf{n}_q \mathbf{n}_q} = \eta(1 - \eta)(\mathbf{H}\mathbf{R}_{\mathbf{xx}}\mathbf{H}^H) + N_o \mathbf{I}$ [33] is the covariance of the quantization noise. Substituting $\mathbf{R}_{\mathbf{n}_q \mathbf{n}_q}$ in (4) yields

$$\gamma_q = (1 - \eta)(\mathbf{H}\mathbf{R}_{\mathbf{xx}}\mathbf{H}^H)(N_o \mathbf{I} + \eta(\mathbf{H}\mathbf{R}_{\mathbf{xx}}\mathbf{H}^H))^{-1}, \quad (5)$$

and finally, in terms of the SNR of the unquantized signal (γ), γ_q can be written as [34]

$$\gamma_q = (1 - \eta)\gamma(\mathbf{I} + \eta\gamma)^{-1} \quad (6)$$

At low SNR, γ_q can be approximated as $(1 - \eta)\gamma$, while at high SNR and for finite bits b , the quantized SNR γ_q is tightly upper bounded by $\min(\frac{1-\eta}{\eta}, \gamma)$. Note that, for very high resolution, $\eta \rightarrow 0$ and γ_q in (6) will be very close to the SNR of the unquantized signal γ . Finally, the achievable rate of the MIMO link with an AQNM signal in (3) is given as

$$C_q = E_{\mathbf{H}} \left[\max_{\mathbf{R}_{\mathbf{xx}}} B \log_2 \left| \mathbf{I} + (1 - \eta)(\mathbf{H}\mathbf{R}_{\mathbf{xx}}\mathbf{H}^H)(N_o \mathbf{I} + \eta(\mathbf{H}\mathbf{R}_{\mathbf{xx}}\mathbf{H}^H))^{-1} \right| \right] \quad (7)$$

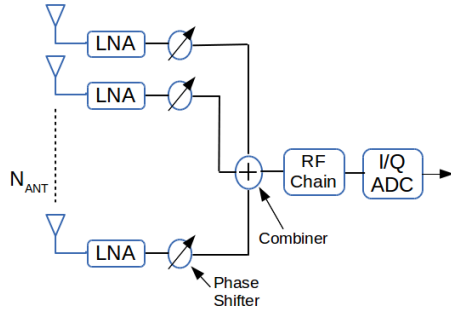


Figure 1. Analog Combiner.

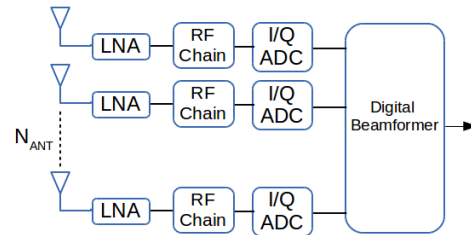


Figure 2. Digital Combiner.

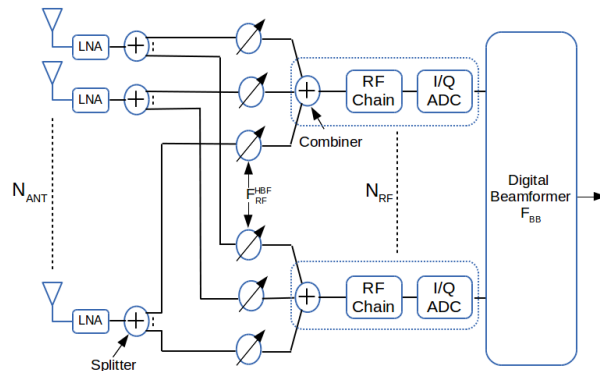


Figure 3. Hybrid Combiner.

III. RECEIVER ARCHITECTURES

This section characterizes the achievable rates in mmW links with three types of receiver architectures featuring quantization. For all three cases, the transmitter architecture is considered to be always fully digital with ideal MIMO processing. We also assume the availability of channel state information (CSI) both at the transmitter and at the receiver and we design the MIMO processing accordingly.

The three architectures are termed Analog, Digital, and Hybrid, and represented in Figures 1, 2 and 3. The difference between the three architectures consists in their different analog processing hardware prior to the ADC, which modifies the total number of RF and ADC units, and the number of digital signal dimensions that may be further processed by digital stages.

A. Analog Combining

The first architecture is Analog Combining, which is motivated by the fact that typically ADCs are considered as the most power-hungry receiver components. Therefore, in this architecture all multiple-antenna processing is performed in the analog domain to minimize power consumption.

The architecture in Figure 1 features one phase shifter per receive antenna and an analog signal adder; together, these devices implement analog beamforming and deliver a scalar combined signal to a one-dimensional RF and ADC chain.

The quantized received signal y_q with AC at the receiver and digital beamforming at the transmitter is given by

$$y_q = (1 - \eta)(\mathbf{w}_r^H \mathbf{H} \mathbf{w}_t x + \mathbf{w}_r^H \mathbf{n}) + \mathbf{n}_q \quad (8)$$

where \mathbf{w}_t represents the digital beamforming vector at the transmitter such that $\|\mathbf{w}_t\|^2 = 1$ and \mathbf{w}_r is the AC vector at the receiver with a constant amplitude per coefficient $|w_{r,i}| = 1/\sqrt{N_r}$ due to its implementation using phase shifters.

The additive quantization noise variance is given by $\eta(1 - \eta)(|\mathbf{w}_r^H \mathbf{H} \mathbf{w}_t|^2 P + N_o)$, where P is the average transmitter power. The ergodic rate maximization problem with AC is given as

$$C_{AC} = \mathbb{E}_{\mathbf{H}} \left[\max_{\mathbf{w}_r, \mathbf{w}_t} B \log_2 \left(1 + \frac{(1 - \eta) |\mathbf{w}_r^H \mathbf{H} \mathbf{w}_t|^2 P}{N_o + \eta |\mathbf{w}_r^H \mathbf{H} \mathbf{w}_t|^2 P} \right) \right] \\ \text{s.t. } |w_{r,i}| = \frac{1}{\sqrt{N_r}}, \quad (9) \\ \|\mathbf{w}_t\|^2 = 1,$$

Due to the fact that CSI is available for each channel realization, and the fact that (9) is a monotonic function of $|\mathbf{w}_r^H \mathbf{H} \mathbf{w}_t|^2$, the maximization of the ergodic rate is achieved by maximizing this beamforming gain independently for each channel realization.

The transmitter beamforming vector, which has fewer constraints, can be simply assigned the value that maximizes the gain for a given value of \mathbf{w}_r . This consists in implementing a matched filter at the transmitter with value $\mathbf{w}_t = \frac{\mathbf{H}^H \mathbf{w}_r}{\|\mathbf{H}^H \mathbf{w}_r\|}$, where the normalization is required to satisfy the transmit power constraint.

By using the matched filter at the transmitter, we can rewrite the problem as finding the receive beamforming vector that maximizes $|\mathbf{w}_r^H \mathbf{H}|^2$. If \mathbf{w}_r had no per-coefficient amplitude constraints, the optimal receive beamforming would be the eigenvector \mathbf{u}_{\max} associated with the largest singular value σ_{\max} of matrix \mathbf{H} , i.e.,

$$\mathbf{u}_{\max} = \arg \max_{\mathbf{w}_r \in \mathbb{C}^{N_r}} |\mathbf{w}_r^H \mathbf{H}|^2, \quad (10)$$

However, since the analog scheme can only alter the phase of a constant-amplitude beamforming vector, the exact optimal analog beamforming vector is, in turn, expressed as

$$\mathbf{w}_r^* = \arg \max_{\mathbf{w}_r: |w_r^i| = 1/\sqrt{N_r}} |\mathbf{w}_r^H \mathbf{H}|^2. \quad (11)$$

Finally, due to the fact that the problem in (11) is more difficult, in our model we consider that the receiver instead settles for an approximate solution consisting in the projection of the unconstrained optimal beamforming vector \mathbf{u} from (10) to the nearest point over the space of constant-amplitude vectors, i.e.,

$$\tilde{\mathbf{w}}_r^H = \frac{1}{\sqrt{N_r}}(e^{\angle u_{\max}^1}, e^{\angle u_{\max}^2}, \dots, e^{\angle u_{\max}^{N_r}})^T \quad (12)$$

B. Digital Combining

The second architecture is Digital Combining, which is motivated by the fact that digital MIMO processing has in general fewer constraints and can achieve higher gains. Therefore, in this architecture all multiple-antenna processing is performed in the digital domain to maximize the rate. The architecture in Figure 2 features no analog processing; each antenna directly delivers its received signal to a dedicated RF and ADC chain. A quantized signal with N_r dimensions is processed by a Digital MIMO processor that allows the spatial multiplexing of up to $N_s \leq \min(N_t, N_r)$ symbol streams. The quantized received signal with DC is given as

$$\mathbf{y}_q = (1 - \eta)(\mathbf{W}_r^H \mathbf{H} \mathbf{W}_t \mathbf{x} + \mathbf{W}_r^H \mathbf{n}) + \mathbf{W}_r^H \mathbf{n}_q \quad (13)$$

where \mathbf{W}_r and \mathbf{W}_t are the digital combining and beamforming matrices, respectively. Note that, as combining is performed after quantization, the DC matrix also multiplies the quantization noise. To calculate the supremum of the achievable rate with DC, we design the beamforming and combining matrices corresponding to the singular value decomposition of the channel matrix i.e., $\mathbf{H} = \mathbf{U}\Sigma\mathbf{V}^H$, where \mathbf{U} and \mathbf{V} are the left and right singular matrices, respectively, and Σ is a diagonal matrix with the singular values. Now, by applying a transmit beamforming matrix $\mathbf{W}_t = \mathbf{V}$ and a receive combining matrix $\mathbf{W}_r = \mathbf{U}^H$, Eq. (13) can be written as

$$\mathbf{y}_q = (1 - \eta)(\mathbf{U}^H \mathbf{U} \Sigma \mathbf{V}^H \mathbf{V} \mathbf{x} + \mathbf{U}^H \mathbf{n}) + \mathbf{U}^H \mathbf{n}_q = (1 - \eta)(\Sigma \mathbf{x} + \mathbf{U}^H \mathbf{n}) + \mathbf{U}^H \mathbf{n}_q \quad (14)$$

Finally, we allocate the transmit power across the singular values of Σ using the water filling algorithm, and the rate with DC results in

$$C_{DC} = E_{\mathbf{H}} \left[\max_{\mathbf{R}_{\mathbf{xx}}} B \log_2 \det \left[\mathbf{I} + (1 - \eta) \Sigma \mathbf{R}_{\mathbf{xx}} \Sigma^H (N_o \mathbf{I} + \eta \mathbf{U}^H \text{diag}(\mathbf{U} \Sigma \mathbf{R}_{\mathbf{xx}} \Sigma^H \mathbf{U}^H) \mathbf{U})^{-1} \right] \right] \quad (15)$$

where the input covariance matrix that maximizes the rate for each channel realization, $\mathbf{R}_{\mathbf{xx}}$, appears also in the noise term. This means that with b bits the optimal $(\mathbf{R}_{\mathbf{xx}})_b^*$ is not exactly the same as the optimal for the unquantized channel, $(\mathbf{R}_{\mathbf{xx}})_\infty^*$, calculated using the water-filling

algorithm. However, as the number of quantization bits grows we have $\lim_{b \rightarrow \infty} (\mathbf{R}_{\mathbf{xx}})_b^* = (\mathbf{R}_{\mathbf{xx}})_\infty^*$. Therefore, in our DC model we use a near-optimal water-filling input distribution that lower bounds the achievable rates for DC and approaches the optimal as b increases.

At low SNR, the waterfilling algorithm allocates all the power to the maximum singular value, and therefore the beamforming and combining vectors are just the right and left singular vectors (\mathbf{v}_{\max} and \mathbf{u}_{\max}) corresponding to the maximum singular value, respectively. This shows how the optimal number of spatial streams, N_s , may be smaller than $\min(N_t, N_r)$; compared with AC, which only provides beamforming gain, DC can provide the advantages of both spatial multiplexing gains at high SNR and beamforming power gains at low SNR. Although DC achieves a rate similar to AC at low SNR as the water filling algorithm concentrates all the transmitted power into a single eigenvector corresponding to the maximum eigenvalue, the DC rate is always better than AC, due to the fact that the DC architecture does not impose constant-amplitude constraints in the receive combining vector. The rate with DC at low SNR, with $\frac{PE[|\mathbf{H}|^2]}{N_0} \ll 1$, is given as

$$C_{DC} \stackrel{\frac{PE[|\mathbf{H}|^2]}{N_0} \ll 1}{\simeq} E_{\mathbf{H}} \left[B \log_2 \left(1 + \frac{(1-\eta)|\mathbf{u}_1^H \mathbf{H} \mathbf{v}_1|^2 P}{N_o + \eta |\mathbf{u}_1^H \mathbf{H} \mathbf{v}_1|^2 P} \right) \right] \quad (16)$$

C. Hybrid Combining

The third architecture is Hybrid Combining, which is motivated by the high rate and the low power consumption of DC and AC architectures, respectively, and tries to strike a balance between the two. The architecture in Fig. 3 features an analog processing stage with multiple banks of phase shifters, each with an independent analog adder, RF and ADC chain. The analog processing reduces the dimensions of the received signal to a number N_{RF} greater than one (analog case) but smaller than N_r (digital case). The analog processed signal with N_{RF} dimensions is quantized and digitally processed allowing the spatial multiplexing of up to $N_s \leq \min(N_t, N_{RF}) \leq N_r$ symbol streams. The quantized signal with HC is given by

$$\mathbf{y}_q = (1-\eta)(\mathbf{W}_{BB}^H \mathbf{W}_{RF}^H \mathbf{H} \mathbf{W}_t \mathbf{x} + \mathbf{W}_{BB}^H \mathbf{W}_{RF}^H \mathbf{n}) + \mathbf{W}_{BB}^H \mathbf{n}_q \quad (17)$$

where \mathbf{W}_{RF} and \mathbf{W}_{BB} are the RF and the baseband combining vectors, respectively. Let $\mathbf{n}_e = \mathbf{W}_{RF}^H \mathbf{n}$ represent equivalent receiver noise, $\mathbf{H}_e = \mathbf{W}_{RF}^H \mathbf{H}$ represent an $N_{RF} \times N_t$ equivalent channel matrix, and $\mathbf{H}_e = \mathbf{U} \Sigma \mathbf{V}^H$ represent its singular value decomposition. The digital baseband

combiner may be set to $\mathbf{W}_{BB} = \mathbf{U}^H$, and its corresponding transmit beamformer to $\mathbf{W}_t = \mathbf{V}$, which leaves the quantized signal in (17) written as

$$\mathbf{y}_q = (1 - \eta)(\Sigma \mathbf{x} + \mathbf{U}^H \mathbf{n}_e) + \mathbf{U}^H \mathbf{n}_q \quad (18)$$

Similar to the analog case, the design of \mathbf{W}_{RF} is affected by the phase shifter with constant amplitude constraints. The unconstrained optimization should maximize the result of a water-filling over the N_{RF} singular values of the equivalent channel $\mathbf{H}_e = \mathbf{W}_{RF} \mathbf{H}$, and results in the following optimization problem

$$\mathbf{W}_{RF}^{ideal} = \arg \max_{\mathbf{W}_{RF} \in \mathbb{C}^{N_r \times N_{RF}}} \max_{\sum p_i = P} \sum_{\mathcal{S}(\mathbf{W}_{RF} \mathbf{H})} \sigma_i^2 p_i, \quad (19)$$

where $\mathcal{S}(\mathbf{W}_{RF} \mathbf{H})$ denotes the spectrum of the matrix and σ_i^2 is the i^{th} eigenvalue. However, the analog processors can only alter the phase of constant-amplitude values of \mathbf{W}_{RF} . This, in turn, is expressed as

$$\mathbf{W}_r^* = \arg \max_{\mathbf{W}_{RF}: |W_r^{ij}| = 1/\sqrt{N_r}} \max_{\sum p_i = P} \sum_{\mathcal{S}(\mathbf{W}_{RF} \mathbf{H})} \sigma_i^2 p_i. \quad (20)$$

However, the latter optimization poses a number of issues. First, the selection of the best beamforming matrix in (20) is not a linear problem because the target function contains a power allocation. Second, the formulation of (20) satisfies the norm constraints but does not satisfy the semi unitary constraints of the hardware. Therefore, to satisfy both norm and semi unitary constraints we select \mathbf{W}_{RF} using a practical approximate solution by using an alternate projection method [35]. The procedure is summarized in Algorithm 1 and consists in an alternate projection iterative method. The algorithm starts by generating a semi unitary matrix \mathbf{W}_{SU} , which is equal to the first N_{RF} vectors of the left singular matrix of \mathbf{H} . In the next step, the RF combining matrix $\tilde{\mathbf{W}}_{RF}$ is generated such that the corresponding elements have similar phase as that of \mathbf{W}_{SU} but with constant normalized amplitude. In the next step, $\tilde{\mathbf{W}}_{RF}$ is again projected back to the semi unitary matrix \mathbf{W}_{SU} . The process continues until the algorithm converges (i.e., the matrix coefficients change less than a small step threshold value). The convergence properties of the algorithm are studied in [35]. This results in a similar \mathbf{y}_q as obtained with DC in (14). However, \mathbf{U} has a dimension of N_{RF} instead of N_r , due to the limited number of RF chains. The achievable rate with HC is given as

$$C_{HC} = E_{\mathbf{H}} \left[\max_{\mathbf{R}_{xx}} B \log_2 \det \left| \mathbf{I} + (1 - \eta) \Sigma \mathbf{R}_{xx} \Sigma^H (N_o \mathbf{I} + \eta \mathbf{U}^H \text{diag}(\mathbf{U} \Sigma \mathbf{R}_{xx} \Sigma^H \mathbf{U}^H) \mathbf{U})^{-1} \right| \right] \quad (21)$$

Algorithm 1 Alternate projection method for design RF combining matrix for HC

 Initialize $\mathbf{W}_{SU} = [\mathbf{u}_1 \dots \mathbf{u}_{N_{RF}}] \in \mathbf{U}$, where $\mathbf{H} = \mathbf{U}\Sigma\mathbf{V}^H$
while not converging **do**

$$[\tilde{\mathbf{W}}_{RF}]_{ij} = \frac{1}{\sqrt{N_r}} \exp(j\angle[\mathbf{W}_{SU}]_{ij}), \forall i, j$$

$$\mathbf{W}_{SU} = (\tilde{\mathbf{W}}_{RF} \tilde{\mathbf{W}}_{RF}^*)^{-\frac{1}{2}} \tilde{\mathbf{W}}_{RF}$$

end while

Although the two rate expressions for DC and HC are similar, the rate of HC is upper bounded by the rate of DC due to the fact that the selection of \mathbf{W}_{RF} is subject to a constant amplitude constraint associated with the analog combiners. We also point out that in our formulation we use infinite-resolution phase shifters for AC or HC, whereas in practice only finite-resolution quantized phase steps are employed. Therefore, the rates achieved following (9) and (21) are in fact greater than what would be obtained with a quantized phase shifter constraint.

Lastly, note that as was the case with DC, the input covariance matrix that maximizes the HC rate with b bits, $(\mathbf{R}_{xx})_b^*$, is not that which is calculated with the water-filling algorithm, $(\mathbf{R}_{xx})_\infty^*$. This means that our implementation using water-filling is slightly lower than the maximal rates achievable with a HC scheme in (21). Nevertheless, our comparison between DC and HC remains valid due to the fact that we apply a simplification of the same type to both models and, since the simplification is worse for low b and we are primarily interested in when DC with a few bits outperforms HC with many bits, in fact this simplification is slightly skewed in favor of HC.

D. Spectral Efficiency Calculation

We compare the average achievable rates for AC, DC and HC mmW links as a function of the number of ADC bits. Figures 4 and 5 show the rate vs ADC bits when the number of propagation clusters and paths per cluster (N_c, N_p) are $(1, 1)$ for an ideal rank 1 channel, and when they are $(Poisson(1.8), 20)$ for a more realistic channel model as in [15], respectively. We evaluate the theoretical integrals for the averages of Eqs. (9), (15), and (21) using the Monte-Carlo numerical integration method with 1000 realizations of the channel distribution per point. We consider $N_t = 64$, $N_r = 16$, $N_{RF} = 4$, bandwidth $B = 1$ GHz, and a total transmit power of 30 dBm. We show results for -20 and 0 dB SNR not including antenna gain, which corresponds to an approximate communication range of 100 m for NLOS and LOS, respectively.

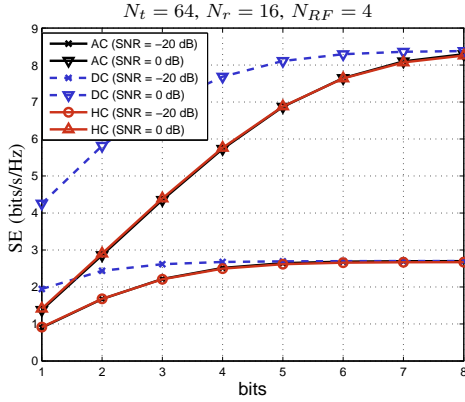


Figure 4. Achievable rate vs ADC bits comparison for AC, DC and HC schemes for $(N_c, N_p) = (1, 1)$.

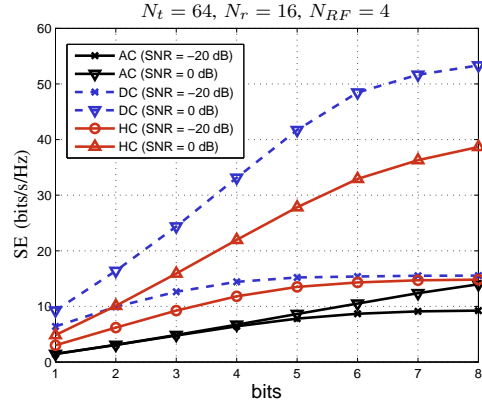


Figure 5. Achievable rate vs ADC bits comparison for AC, DC and HC schemes for $(N_c, N_p) = (Poisson(1.8), 20)$.

In both figures we can see that, for all architectures, the rate grows up to a certain number of ADC bits and saturates afterwards, so that a further increase in b does not improve the SNR of the quantized signal. This threshold appears later when the unquantized signal SNR (γ) is higher, as in this case more bits are necessary to reach saturation.

The results show that the DC architecture outperforms the other schemes for both cases of propagation paths. This is due to the fact that DC does not have constant amplitude constraints in the beamforming coefficients. Moreover, in the case of $(N_c, N_p) = (1, 1)$, i.e., if the channel has rank 1, spatial multiplexing is not possible, and AC can perform similarly to HC or DC, but only for a high number of ADC bits. In the opposite case, for $(N_c, N_p) = (Poisson(1.8), 20)$, AC achieves significantly lower rates at high SNR because it cannot exploit spatial multiplexing, unlike HC and DC. At low SNR, AC is closer to HC and DC because the water-filling algorithm concentrates all the power in one eigenvalue and there is no multiplexing gain anyways. This shows that the appeal of AC schemes is strongest for single-path sparse propagation environments and low-SNR links. Finally, even though HC exploits spatial multiplexing, its rate is always slightly lower than DC due to the constant amplitude constraint of the RF combining matrix (\mathbf{W}_{RF}) and also to the fact that DC's spatial multiplexing gain is not upper bounded by N_{RF} .

IV. ENERGY EFFICIENCY ANALYSIS

Looking only at rate, the straightforward choice for a mmW receiver design would be a fully digital architecture (i.e., DC), which can exploit the maximum advantages of both beamforming and spatial multiplexing techniques, and thus always outperforms AC and HC. However, generally, these advantages of DC are tied to a higher power consumption at the receiver. Thus,

TABLE III
POWER CONSUMPTION OF EACH DEVICE

Device	Notation	Value
Low Noise Amplifier (LNA) [36]	P_{LNA}	39 mW
Splitter	P_{SP}	19.5 mW
Combiner [36]	P_C	19.5 mW
Phase shifter [37], [38]	P_{PS}	2 mW or 0
Mixer [39]	P_M	16.8 mW
Local oscillator [27]	P_{LO}	5 mW
Low pass filter [27]	P_{LPF}	14 mW
Base-band amplifier [27]	$P_{BB_{amp}}$	5 mW
ADC	P_{ADC}	$cB2^b$

TABLE IV
ADC POWER PER SAMPLE AND PER LEVEL, c

Scenario	Value	Generation
LPADC	5 fJ/step/Hz	Ideal future value
IPADC	65 fJ/step/Hz	Intermediate Power (Recently proposed)
HPADC	494 fJ/step/Hz	State of the art

although DC results in the maximum achievable rates, it may not always be an energy efficient receiver option.

In particular, in the large bandwidth operation expected at mmW, the ADC is usually considered to be the most power hungry block and thus the power consumption of DC is penalized by its large number of ADCs (N_{ADC}), equal to twice the number of receive antennas. In comparison, AC, only requiring 2 ADCs, would be the the least power consuming scheme, and HC, requiring $N_{ADC} = 2 \times N_{RF}$, is generally assumed to have a power consumption in-between AC and DC.

Nonetheless, looking only at the ADC, and disregarding the power consumption of other analog components that are not necessary for DC, may be misleading. Particularly, if the power consumption of phase shifters and analog combiners is non-negligible, HC may be penalized due to the fact that it requires a large number (up to N_{RF}) of both analog blocks and ADCs at the same time.

In this section we develop a detailed study of the EE of the three architectures, defined as

$$EE = \frac{C_q}{P_{Tot}} \quad (22)$$

where C_q is the achievable rate of the quantized signal corresponding to different combining schemes and P_{Tot} is the total power consumption of the mmW receiver design corresponding to AC, DC and HC architectures.

A. Power Consumption Model

The devices required to implement each mmW receiver architecture are displayed in Figures 1, 2 and 3, respectively. The total power consumption P_{Tot} of each scheme is evaluated by the

following expressions

$$P_{Tot}^{AC} = N_r(P_{LNA} + P_{PS}) + P_{RF} + P_C + 2P_{ADC} \quad (23)$$

$$P_{Tot}^{HC} = N_r(P_{LNA} + P_{SP} + N_{RF}P_{PS}) + N_{RF}(P_{RF} + P_C + 2P_{ADC}) \quad (24)$$

$$P_{Tot}^{DC} = N_r(P_{LNA} + P_{RF} + 2P_{ADC}) \quad (25)$$

where P_{RF} represents the power consumption of one RF chain, given by

$$P_{RF} = P_M + P_{LO} + P_{LPF} + P_{BBamp}, \quad (26)$$

and the component power consumptions are detailed in Table III. The power consumption of all components except the ADC is independent of the bandwidth B and the number of bits b , whereas P_{ADC} increases exponentially with b and linearly with B and with the ADC Walden's figure of merit c [40] (the energy consumption per conversion step per Hz).

It must be noted that, depending on the choice of power values for each component, our model may give a different outcome about whether HC or DC performs better. For example, if we used a very high ADC Walden's figure of merit, e.g., 12.5 pJ/step/Hz as in [41], we would heavily penalize DC, giving an unfair advantage to HC. Likewise, if we considered a very high Phase Shifter power consumption, such as 19.5 mW in [36], we would be similarly giving an unfair advantage to DC.

In this paper we have selected two reasonable component power consumption models that we approximately identify with two generations of technology, current and upcoming. The considered ADCs Walden's figure of merit is detailed in Table IV.

- The High Power ADC (HPADC) model is based on an existing device that supports sampling at Gs/s and has been referenced in related literature such as [24]. In order to give Phase Shifters appropriate power consumption values, we pair the existing ADC model with an existing PS model with $P_{PS} = 2$ mW, referenced in [37].
- The Low Power ADC (LPADC) model considers a likely future best-case scenario deduced from the hardware survey in [42]. Likewise, we pair this "best case future scenario" with a best case phase shifter model, with negligible power consumption ~ 0 mW, as in [38]³.

³ADC power values are rapidly changing, and we consider the extreme cases of well-established HPADC [24] and future LPADC [42]. Very recently a new Intermediate Power ADC (IPADC) has been proposed in [43]. Given this dynamic situation, we complement our study with a method and a web visualization tool so that researchers can reproduce the charts and easily bring in the advances in ADC technology to our model [14].

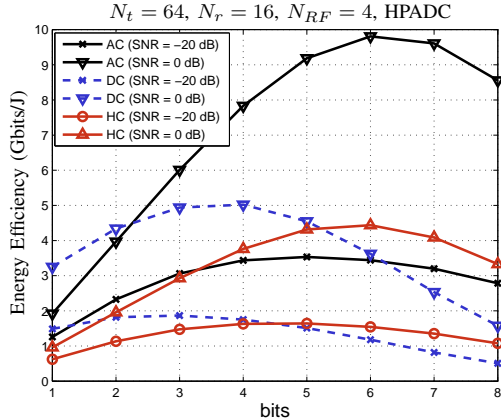


Figure 6. EE vs. ADC bits comparison for AC, DC and HC schemes for $(N_c, N_p) = (1, 1)$.

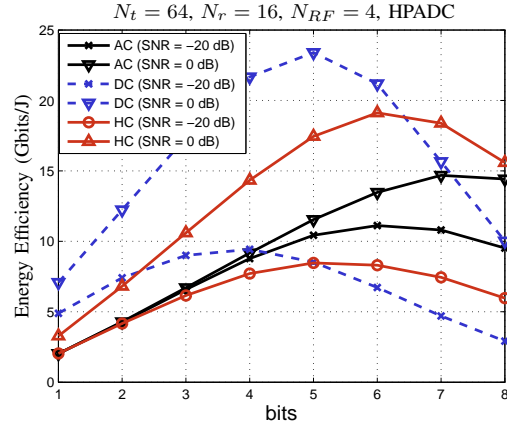


Figure 7. EE vs. ADC bits comparison for AC, DC and HC schemes for $(N_c, N_p) = (Poisson(1.8), 20)$.

B. Energy Efficiency Calculation

We analyze the EE of each receiver architecture using the power values per component defined in Tables III and IV. We show the EE vs the number of ADC bits in the HPADC scenario for two SNR values, -20 dB and 0 dB, when the number of propagation clusters and paths per cluster (N_c, N_p) are $(1, 1)$ and $(Poisson(1.8), 20)$, in Figures 6 and 7, respectively. In this analysis we have considered a mmW antenna array with $N_t = 64$, and $N_r = 16$, a hybrid scheme with $N_{RF} = 4$, and a channel with bandwidth $B = 1$ GHz.

The plots show that all combining schemes have an optimal number of ADC bits which results in a maximum EE. Note that this optimal point is influenced by both the flat saturation of the rate as a function of b , which depends on SNR, and by the exponential increase in ADC power consumption with b .

Comparing the three receiver architectures, we note that surprisingly DC offers the highest EE of the three schemes with a HPADC model in a dense multi-path environment with high SNR (Figure 7 for 0 dB) whereas AC achieves highest EE in case of a single cluster/single path scenario or low SNR (Figure 6 and Figure 7 for -20 dB). Note that DC EE decays rapidly when b is beyond the optimal, and thus HC outperforms DC when both have a high number of bits. However, it is incorrect to extrapolate from this that HC always outperforms DC. Also note that in Fig. 7 at high SNR, DC has higher EE than other schemes up to 6 bits, and this number of bits is high enough to avoid any noticeable degradation in SE (see Fig. 5). We also mention that the number of ADC bits also affects the choice of the modulation scheme, for instance ADCs with only 1 or 2 bits cannot support higher order modulation schemes such as 64-QAM, which

may also result in a reduction of the achievable rate compared to a high resolution ADC.

Comparing the SNR across the same architecture, we observe that the rate saturation occurs at a larger number of bits when SNR is higher, and therefore the optimal number of bits increases with SNR. Moreover, when the SNR is low, AC has better performance than HC and DC, due to the fact that at low SNR the water-filling algorithm focuses all the power in a single singular value of the channel and HC and DC do not exploit spatial multiplexing gains.

It must be noted that the DC receiver with highest EE and the receiver with the highest SE do not have the same number of bits. For this reason, in the next section we develop a framework to compare receivers in the two dimensions.

V. TRADE-OFF ANALYSIS AND EFFECT OF PARAMETERS

In this section, we develop the full two-dimensional SE and EE comparison of DC, HC, and AC receiver architectures. To this end, we create comparison charts that represent the EE and the SE of each receiver design, making it possible to study the choice of appropriate receiver schemes for different needs, and to observe the trade-off between the two metrics. We write EE as a function of SE as

$$\begin{aligned}
 EE &= \frac{B \times SE}{P_o + P_a N_r + 2N_r P_{ADC}} \stackrel{(a)}{=} \frac{SE}{(P_o + P_a N_r)/B + 2N_r c 2^b} \\
 &\stackrel{(b)}{\simeq} \frac{SE}{(P_o + P_a N_r)/B + 2N_r c \sqrt{\frac{2}{\pi\sqrt{3}} \frac{\gamma}{(1+\gamma)2^{-SE}-1}}}
 \end{aligned} \tag{27}$$

where we denote by P_o the power consumption of all fixed receiver components and by P_a the power consumption of all per-antenna analog receiver components except ADCs, (a) comes from $P_{ADC} = cB2^b$ in Table III and (b) comes from combining (6) and $\eta \simeq \frac{\pi\sqrt{3}}{2}2^{-2b}$.

This expression displays three behavior regimes:

- 1) At $(P_o + P_a N_r)/B \gg 2N_r c \sqrt{\frac{2}{\pi\sqrt{3}} \frac{\gamma}{(1+\gamma)2^{-SE}-1}}$, where EE grows linearly with SE.
- 2) At $(P_o + P_a N_r)/B \simeq 2N_r c \sqrt{\frac{2}{\pi\sqrt{3}} \frac{\gamma}{(1+\gamma)2^{-SE}-1}}$, where EE is maximum.
- 3) At $(P_o + P_a N_r)/B \ll 2N_r c \sqrt{\frac{2}{\pi\sqrt{3}} \frac{\gamma}{(1+\gamma)2^{-SE}-1}}$, where EE decreases exponentially with SE.

In order to know whether a receiver architecture is better or worse than another, we must look at the SE and EE around the transition point in regime 2. For the sake of a simple discussion let us consider $P_o \ll N_r P_a$ and focus on the term $N_r P_a$. We can calculate a point in the transition regime \tilde{SE} by solving the equation $P_a/B = 2c \sqrt{\frac{2}{\pi\sqrt{3}} \frac{\gamma}{(1+\gamma)2^{-SE}-1}}$, which may be rewritten as $\tilde{SE} = \log_2 \frac{\gamma+1}{\gamma + \frac{2}{\pi\sqrt{3}} \left[\frac{P_a}{2Bc} \right]^2}$. Ideally we would be interested in finding the true optimal that maximizes

the EE in (27), denoted by SE^* . However, since SE^* belongs to regime 2 by definition, we know that its value must be close to \tilde{SE} . Therefore we can obtain some qualitative insights about the behavior of SE^* by analyzing the approximate value \tilde{SE} .

Let us compare two receivers with SNRs $\gamma^{(1)}$ and $\gamma^{(2)}$ and analog RF chain power consumptions $P_a^{(1)}$ and $P_a^{(2)}$. Let us define a difference in parameters $\Delta P_a^2 = (P_a^{(2)})^2 - (P_a^{(1)})^2$, and define the required SNR difference $\Delta\gamma^* = \gamma^{(2)} - \gamma^{(1)}$ such that receiver #2 achieves a greater or equal value in \tilde{SE} than receiver #1.

$$\Delta\gamma^* = \frac{(\gamma^{(1)} + 1)((P_a^{(2)})^2 - (P_a^{(1)})^2)}{(P_a^{(1)})^2 - \frac{\pi\sqrt{3}}{2}(Bc)^2} \quad (28)$$

where we observe that if Walden's figure of merit c is low, a higher SNR is required to achieve the same SE in a receiver with the optimal EE. However, if c is high, $\Delta\gamma^*$ changes sign and becomes negative. This means that the value $\tilde{SE} \simeq SE^*$ to maximize EE decreases, and that fewer bits are used in the optimal ADC configuration. But since the use of fewer bits increases the quantization noise, such a system can operate with a lower unquantized SNR without losing performance. In summary, switching from DC to HC can produce a significant gain or a significant loss depending critically on the component parameters, SNR, and preference of EE over SE. This calls for an analytic framework that optimizes both EE and SE at the same time.

For each architecture, we plot a curve in a chart representing the evolution of its SE versus EE performance as the number of ADC bits b increases from 1 to 8, at increments of 1. The highest points in the chart correspond to highest SE and the rightmost points in the chart correspond to highest EE. Generally speaking, the closer a point to the top-right corner, the better. However, this guideline is not precise enough to fully describe the needs of receiver designers. Thus, we construct a multi-objective utility optimization interpretation of the charts that allows to quantitatively describe all the points of interest in the graph. For this we consider a free parameter $\alpha \in [0, 1]$ that represents the receiver designer's preference between higher EE and higher SE. The "receiver utility" according to the designer's preference can be expressed and maximized as

$$U = \max_{\{HC, DC, AC\}} \max_{b \in \{1 \dots 8\}} \alpha EE + (1 - \alpha) SE \quad (29)$$

Clearly, with $\alpha = 0$ the above problem maximizes SE, and with $\alpha = 1$ it maximizes EE. Moreover, the above problem is easy to solve exhaustively due to the small size of the exploration set, so we can obtain the solution for all values in the range $\alpha \in [0, 1]$. The set of solutions obtained for all values in the range of α correspond to all the receiver designs that designers

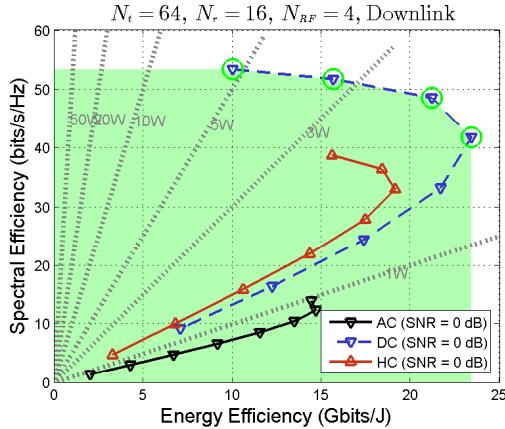


Figure 8. SE vs. EE comparison in high SNR regime for AC, DC and HC schemes for a Downlink scenario with a HPADC model. The optimal receiver configurations for different values of α are the solutions of (29) highlighted with a green circle in the figure.

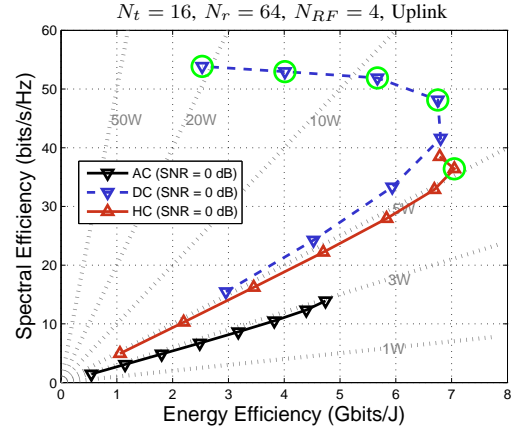


Figure 9. SE vs. EE comparison in high SNR regime for AC, DC and HC schemes for an Uplink scenario with a HPADC model. The optimal receiver configurations for different values of α are the solutions of (29) highlighted with a green circle in the figure.

with different preferences would choose. Hence, receivers not in the set of feasible solutions would never be of use. In the following SE-vs-EE charts, we have highlighted the points that are possible utility maximization solutions with a circle.

In this analysis, we observe the SE vs EE trade-off between AC, HC and DC for both the Downlink and the Uplink scenarios. We first compare the performance of different beamforming schemes both in the high and in the low SNR regimes. We then investigate the dependence of the SE vs EE trade-off results on the component parameters (ADC and the phase shifter power consumption). Finally, we study how the behavior of HC varies with a change in N_{RF} .

A. Uplink-Downlink differences at high SNR

We now investigate the SE vs EE trade-off for AC, DC and HC schemes considering both the Uplink and the Downlink scenarios. For both scenarios, we set $(N_c, N_p) = (Poisson(1.8), 20)$, and $N_{RF} = 4$. For the Downlink, we set $N_t = 64$ and $N_r = 16$, whereas for the Uplink, $N_t = 16$ and $N_r = 64$. Figures 8 and 9 show the SE vs EE trade-off in the high SNR regime for the Downlink and the Uplink scenarios, respectively. In the charts we observe that as b is increased, the curves first reach upward and right, and then wrap around and EE returns to the left corner while SE continues increasing. This is consistent with the analysis of (27).

Each curve can be interpreted as an “achievable region” where receivers of each type can operate. The larger the area covered by a curve, the more versatile the corresponding receiver design. Moreover, the points maximizing (29) for different values of α are highlighted.

Note that the number of bits that maximize SE may not maximize EE. For instance, in Figure 8 the circled point in the left top corner that maximizes SE ($\alpha = 0$) corresponds to $b = 8$, whereas the circled point in the right top corner that maximizes EE ($\alpha = 1$) corresponds to $b = 5$. Notice also that the optimal number of bits for different combining schemes may not be the same, i.e., AC, HC, and DC achieve maximum EE with $b = 7, 6$ and 5 , respectively.

In Fig. 8, we consider the Downlink case, and the highlighted green points represent solutions of (29). Using this set of “best receivers” as a frontier, we can mark a green shadowed area containing all values of EE and SE that are feasible with some receiver. The region in white outside the green boundary represents pairs of values (SE,EE) that cannot be simultaneously achieved by any of the receiver models. We observe that DC is the only architecture that touches the boundary, which means that DC dominates the other schemes and any feasible pair (SE,EE) can be achieved with DC with different numbers of bits. Particularly, DC with 4 or 5 bits consumes lower power than the HC scheme with any number of bits, while also achieving higher SE. Note that in the rest of the figures we will omit the shaded green area for visibility, but the same interpretation of (29) remains valid for all the charts in this paper.

The Downlink case is favorable to DC because the receiver is equipped with only $N_r = 16$ antennas. The power consumption increases in Uplink where the receiver has $N_r = 64$ antennas. This increase affects all schemes but is more severe for DC. In the Uplink, HC with 6-8 bits achieves better (or equivalent) EE than DC with any number of bits. However, in the bi-dimensional utility optimization, (29) with $\alpha = 1$, only HC with 7 bits is actually selected (highlighted in green). When $\alpha > 0$, representing that the designer preference is to jointly maximize the utility sum of EE and SE, DC is used in a wide range of cases from the highest SE ($b = 8$ with $\alpha = 0$), to many points in-between with simultaneously good EE and SE (DC with $b = 5$ or 6 maximizes (29) for mid-range values of $\alpha \in [0, 1]$).

Finally, a constant device power consumption reference grid has been added to the chart (diagonal dotted lines). For a given power constraint, only points below the corresponding rule in the grid may be selected. In Downlink, only AC is a viable receiver below 1 W, whereas above 1 W DC outperforms the other schemes. In Uplink, only AC is viable below 3 W. In the range 3 – 5 W, HC presents a better choice. Finally above 5 W, DC outperforms HC again. Thus, surprisingly, DC is a better receiver for both smaller devices (such as a UE with 1 – 3 W) and larger devices (such as a macro cell BS with 6 – 50 W), while HC is better for mid-range

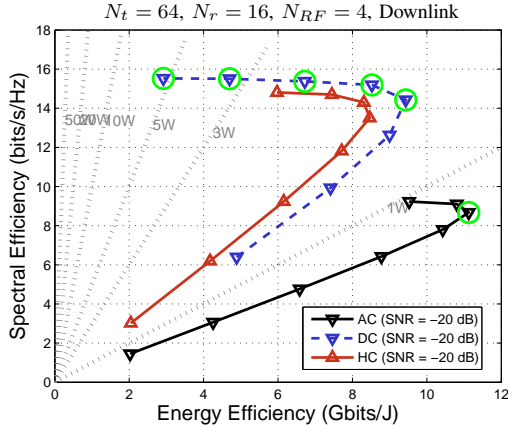


Figure 10. SE vs. EE comparison in low SNR regime for AC, DC and HC schemes with a HPADC model.

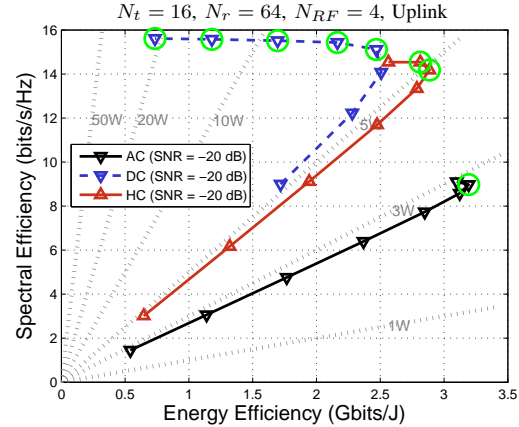


Figure 11. SE vs. EE comparison in low SNR regime for AC, DC and HC schemes with a HPADC model.

power devices (such as a pico cell BS with 3 – 5 W). In devices below 1 W AC should be used. Note that these observations apply only to receivers fabricated with the component consumption values listed in Tables III and IV. Engineers should generate charts for their own components following the example in this paragraph and using the tool available at [14].

Note that we consider high SNR where HC and DC schemes exploit spatial multiplexing gains and are significantly better than AC. Moreover, we consider the HPADC scenario with existing ADC and PS device models. Finally, we only consider $N_{RF} = 4$ in the HC scheme, where an improved EE can be achieved with fewer RF chains, at the cost of SE, and since the channel can support higher spatial dimensions, up to $\min(N_t, N_r) = 16$, the SE can also be augmented by increasing N_{RF} . We investigate the impact of all these parameters in the following sections.

B. Uplink-Downlink differences at Low SNR

The performance trade-off of AC, HC, and DC schemes in low SNR regime for the Downlink and the Uplink is shown in Figures 10 and 11, respectively.

We note that at low SNR (and both in the Downlink and Uplink scenario) water-filling concentrates all the transmitted power in one single strongest dimension (singular value) of the channel. Thus, low-SNR mmWave links with DC or HC plus water-filling behave effectively as rank-1 channels, which were shown in Subsection III-D to achieve very similar SE with AC, HC and DC for a sufficient number of bits. HC and DC cannot exploit any multiplexing gain and have a fairly small difference in SE compared to AC, so AC with its simpler hardware displays much better EE and covers a wider area towards the right.

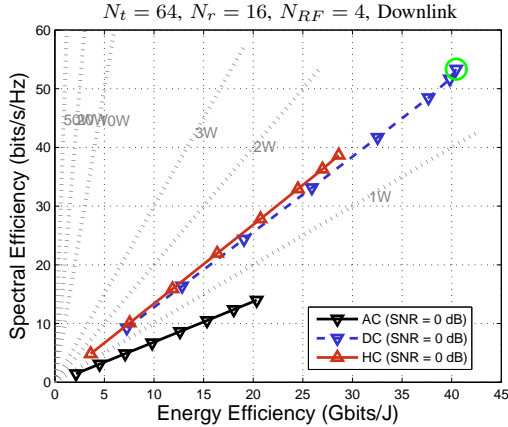


Figure 12. SE vs. EE comparison for AC, DC and HC schemes with a LPADC model and $N_{RF} = 4$ for HC.

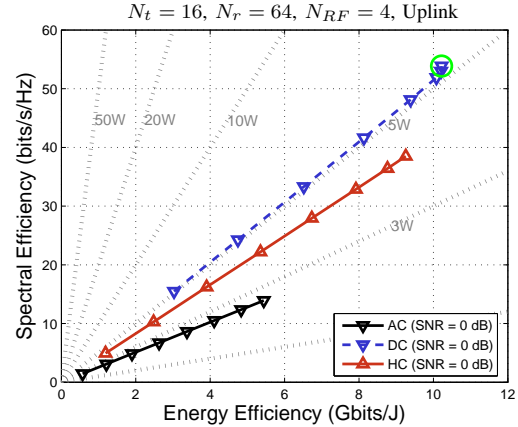


Figure 13. SE vs. EE comparison for AC, DC and HC schemes with a LPADC model and $N_{RF} = 4$ for HC.

The relation between HC and DC follows a similar trend as what was observed in the high SNR case, with the addition of a point of the AC architecture being added to the set of solutions to the multi-objective utility maximization for the maximal values of EE.

Note that in both Downlink and Uplink, by comparing the AC point that achieves the highest EE than the DC or HC, we can observe that choosing AC makes the SE drop by about 40% to increase EE by only about 15%. This drastic difference highlights the importance of performing comparisons in a two-dimensional chart as we propose. Moreover, as we mentioned earlier, the results in these pictures apply only to the parameters in Tables III and IV, and engineers should use the web tool in [14] to produce charts for their parts.

C. Improvement of ADC and Phase Shifter Power Model

Now we study the influence of the component characteristics, and particularly ADC and Phase Shifter power consumption, on the EE vs SE trade-off. We improve the HPADC model employed in Subsection V-A, where we considered state of the art devices with parameters $c = 494$ fJ and $P_{PS} = 2$ mW. Now, we introduce a “reasonable best-case future evolution” set of values considering that the Walden’s figure of merit of the ADC can improve up to 5 fJ [42] and the Phase Shifter power consumption can be reduced almost to zero, $P_{PS} \sim 0$ [38].

Figures 12 and 13 show the SE vs EE plot with the improved component characteristics for the Downlink and the Uplink scenarios, respectively. The charts show that, in general, EE is improved after switching to better ADC and PS parameters. In all schemes, the ADCs power consumption is so low that, in the considered range, the lines do not twist at some optimal number of bits, after which EE starts decreasing. Instead, for $b \leq 8$, EE always increases with

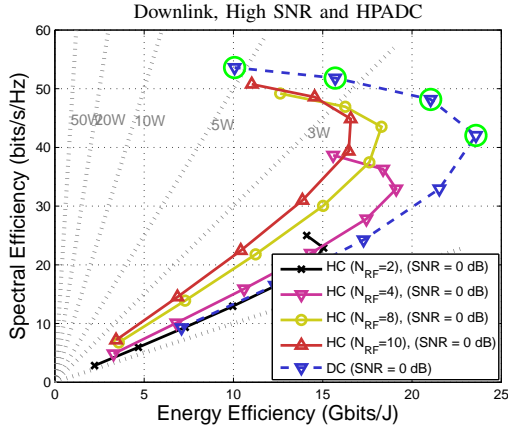


Figure 14. SE vs. EE comparison in high SNR regime for AC, DC and HC schemes for a Downlink scenario with a HPADC model and $N_{RF} = 2, 4, 8, 10$ for HC.

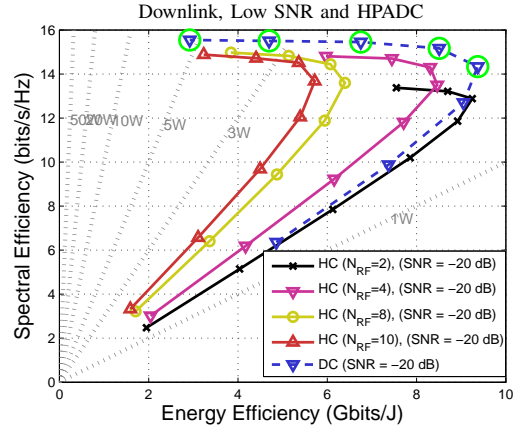


Figure 15. SE vs. EE comparison in low SNR regime for AC, DC and HC schemes for a Downlink scenario with a HPADC model and $N_{RF} = 2, 4, 8, 10$ for HC.

b and the lines are nearly straight. This improvement of EE is better exploited by DC, which dominates HC completely in both Downlink and Uplink according to the utility maximization receiver selection model (29). Note also that when the ADC and PS parameters are improved, the same receiver configuration is selected $\forall \alpha \in [0, 1]$.

If we compare schemes point-to-point for the same number of bits, DC combining always performs better than HC for the same value of b . However, if we make a comparison based on a fixed target SE value, for instance $SE = 40$ bits/s/Hz, then for instance HC with 8 bits can be a better choice than DC with 4 bits in Uplink scenarios.

Note that in the overall power constraint, represented with a grid of diagonal gray lines, we have similar observations than in the previous cases with higher parameters for component power consumption. Namely, AC must be used in Downlink under 1 W and in Uplink under 3 W, and DC can be used in Downlink under 2 W and in Uplink under 5.1 W.

D. RF chains comparison

We now observe the effect on the SE vs EE trade-off for HC as the number of RF chains is changed. Increasing N_{RF} increases SE but also the power consumption, potentially leading to a drop in EE. We compare the performance for both the Downlink and the Uplink while considering both the high and the low SNR regime.

Figures 14 and 15 show the SE vs EE trade-off for the Downlink in the high and low SNR regimes, respectively. At high SNR, an improvement both in SE and in EE is observed by

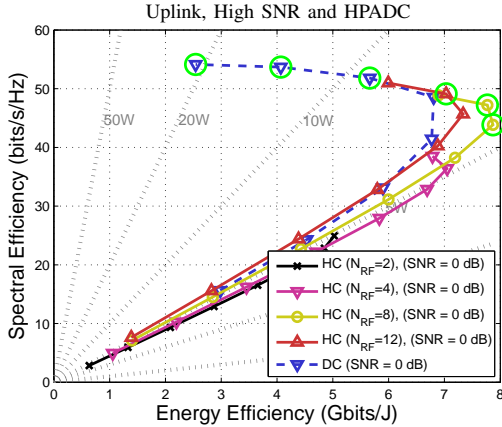


Figure 16. SE vs. EE comparison in high SNR regime for AC, DC and HC schemes for an Uplink scenario with a HPADC model and $N_{RF} = 2, 4, 8, 12$ for HC.

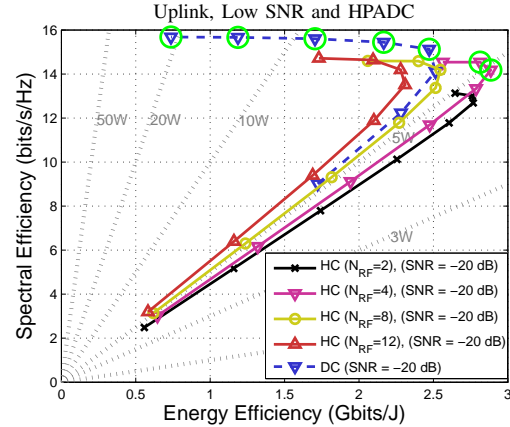


Figure 17. SE vs. EE comparison in low SNR regime for AC, DC and HC schemes for an Uplink scenario with a HPADC model and $N_{RF} = 2, 4, 8, 12$ for HC.

increasing N_{RF} from 2 to 4, i.e., EE is improved from 15 Gbits/J to 19 Gbits/J whereas SE is improved from 22 bits/s/Hz to 32 bits/s/Hz. This is due to the fact that $N_{RF} = 2$ is not sufficient to fully exploit all spatial multiplexing gains available in the channel. Thus, SE increases much more than the power consumption, and as a result EE improves. However, a further increase in N_{RF} only improves SE slightly, whereas EE starts decreasing because a spatial multiplexing gain greater than 4 is much less likely in the random channel with $(N_c, N_p) = (Poisson(1.8), 20)$. Also note that DC is indifferent to the number of RF chains and provides all the best SE and EE multi-objective utility maximization solutions ranging from 5 to 8 bits.

At low SNR, there is no significant spatial multiplexing advantage, and therefore HC seems to perform better with $N_{RF} = 2$. Thus, the optimal number of RF chains is SNR dependent, a troublesome handicap for HC since usually the same hardware is built in all devices and has to be able to operate at different distances in a network. The only scenario where HC achieves EE similar to DC is with $N_{RF} = 2$ and under low SNR, whereas at high SNR the same scheme has a 35% lower EE with HC than with DC. Therefore, another advantage of DC is the ability to adapt digital signal processing to varying channel conditions, which suggests that DC may be a preferable option in the Downlink.

Figures 16 and 17 show the SE vs EE trade-off for the Uplink in the high and low SNR regimes, respectively. Here we considered $N_{RF} = 2, 4, 8$ and 12. The curves for the Uplink follow a similar trend as what was observed for the Downlink scenario, i.e., there is an optimal number of RF chains which maximizes the SE vs EE trade-off and a further increase in N_{RF} decreases EE while SE remains nearly the same. At high SNR, $N_{RF} = 8$ achieves the best SE

vs EE trade-off whereas at low SNR $N_{RF} = 4$ performs best. Note that in the Uplink with either $N_{RF} = 4$ or 8, HC with the optimal N_{RF} achieves better EE than DC in both low and high SNR regimes and the multi-objective utility maximization does switch between DC (when greater SE is preferred) and HC (when greater EE is preferred). Again, the problem of SNR dependence in the selection of the number of RF chains negatively affects the versatility of HC.

VI. CONCLUSIONS

In this work, we studied the spectral and energy efficiency trade-off for analog, digital and hybrid combining schemes. The results show that AC achieves the best EE only in low-SNR or low-rank channels, whereas for any other mmW channel and hardware scenario, DC and HC alternate depending critically on the model parameters and the preference of the receiver designer between maximizing EE or SE.

The ideal scenario for AC, a receiver with low power in a mmW rank-1 channel, may be relevant for systems such as machine-type communications. Even though a rank-1 approximation is moderately accurate in mmW systems, in the median channel a single spatial dimension carries approximately 50% of the energy. This means that AC is a competitive candidate for mmW communications due to its simplicity despite not exploiting fully the $Poisson(1.8)$ dominant transmit dimensions (typically 1-10) for spatial multiplexing and power allocation.

We have shown that the conventional wisdom that HC is preferable over DC is not universally true. Rather, the relationship between DC with few bits and HC is critically determined by mmW channel parameters and component power consumption parameters. The component parameters vary up to two orders of magnitude between different references in the literature, which means that a reproducible comparison framework is needed and example results for any chosen set of parameters cannot hold in general. For this reason, we provide a comprehensive power-consumption comparison method and propose a performance chart technique that allows to choose between HC and DC depending on the given component parameters. We also provided a multi-objective optimization interpretation for the receiver type selection over the bi-dimensional chart, where different preference weights are assigned by the system operator to the SE and EE.

We have also shown that, in one common example of component parameters, if the receiver has a smaller antenna array, or if a subset of the antennas may be turned off to save power, HC does not have an advantage over DC architectures. Particularly, in the Downlink where the receiver is equipped with a low number of antennas, DC achieves better performance than HC,

whereas in the point to point Uplink, HC offers better EE while DC with fewer bits offers a higher utility when SE and EE weights are balanced. However, these results apply to one specific example of component parameters, and engineers should check them with independent charts for the parts available to them.

Moreover, since the mmW scattering is not-so-sparse (e.g., *Poisson*(1.8) clusters), spatial multiplexing gains are critical. DC in the Downlink achieves either a higher rate than HC with similar EE, if HC uses few RF chains; or a similar SE with better EE, if HC uses more RF chains. The optimal number of RF chains which maximizes EE in HC changes with SNR, and a single implementation of a receiver cannot have the optimal value for all distances occurring in a typical network. Also, the measurement-fit mmW channel model we use typically displays rank 1-10 channels, which is the best possible scenario for HC to compete against DC, and yet DC showed advantages. The analysis in the Uplink scenario was, also, more in favor of HC due to the higher number of receive antennas. However, even though HC achieves the highest EE, DC with fewer bits still achieves good EE values with greater SE, potentially being preferable when both characteristics are desired.

While in this paper we focused on spectral and energy efficiency with perfect CSI, channel estimation, fronthaul rates, and receiver size and cost are other important dimensions that need to be considered in future improvements of our work. However, we expect that manufacturing factors may become less important as technology becomes more mature and 5G mmW devices are produced and deployed in very large numbers.

REFERENCES

- [1] W. b. Abbas and M. Zorzi, "Towards an appropriate receiver beamforming scheme for millimeter wave communication: A power consumption based comparison," in *Proceedings of the 22nd European Wireless Conference, 2016*.
- [2] W. bin Abbas, F. Gómez-Cuba, and M. Zorzi, "Millimeter wave receiver comparison under energy vs spectral efficiency trade-off," in *Proceedings of the 23rd European Wireless Conference, 2017*, May 2017, p. To appear.
- [3] T. Rappaport, S. Sun, R. Mayzus, H. Zhao, Y. Azar, K. Wang, G. Wong, J. Schulz, M. Samimi, and F. Gutierrez, "Millimeter wave mobile communications for 5G cellular: It will work!" *IEEE Access*, vol. 1, pp. 335–349, 2013.
- [4] J. G. Andrews, S. Buzzi, W. Choi, S. V. Hanly, A. Lozano, A. C. K. Soong, and J. C. Zhang, "What will 5G be?" *IEEE Journal on Selected Areas in Communications*, vol. 32, no. 6, pp. 1065–1082, Jun 2014.
- [5] F. Boccardi, R. W. Heath, A. Lozano, T. L. Marzetta, and P. Popovski, "Five disruptive technology directions for 5G," *IEEE Communications Magazine*, vol. 52, no. 2, pp. 74–80, Feb. 2014.
- [6] Z. Pi and F. Khan, "An introduction to millimeter-wave mobile broadband systems," *IEEE Communications Magazine*, vol. 49, no. 6, pp. 101–107, Jun. 2011.

- [7] S. Rangan, T. Rappaport, and E. Erkip, "Millimeter-wave cellular wireless networks: Potentials and challenges," *Proceedings of the IEEE*, vol. 102, no. 3, pp. 366–385, Mar. 2014.
- [8] S. Sun, T. S. Rappaport, R. W. Heath, A. Nix, and S. Rangan, "MIMO for millimeter-wave wireless communications: beamforming, spatial multiplexing, or both?" *IEEE Communications Magazine*, vol. 52, no. 12, pp. 110–121, Dec. 2014.
- [9] W. Roh *et al.*, "Millimeter-wave beamforming as an enabling technology for 5G cellular communications: theoretical feasibility and prototype results," *IEEE Communications Magazine*, vol. 52, no. 2, pp. 106–113, Feb. 2014.
- [10] A. Alkhateeb, J. Mo, N. Gonzalez-Prelcic, and R. W. Heath, "MIMO precoding and combining solutions for millimeter-wave systems," *IEEE Communications Magazine*, vol. 52, no. 12, pp. 122–131, Dec. 2014.
- [11] O. E. Ayach, S. Rajagopal, S. Abu-Surra, Z. Pi, and R. W. Heath, "Spatially sparse precoding in millimeter wave MIMO systems," *IEEE Transactions on Wireless Communications*, vol. 13, no. 3, pp. 1499–1513, Mar. 2014.
- [12] J. Mo and R. W. Heath, "Capacity analysis of one-bit quantized MIMO systems with transmitter channel state information," *IEEE Transactions on Signal Processing*, vol. 63, no. 20, pp. 5498–5512, Oct. 2015.
- [13] S. Jacobsson, G. Durisi, M. Coldrey, U. Gustavsson, and C. Studer, "One-bit massive MIMO: Channel estimation and high-order modulations," in *2015 IEEE International Conference on Communication Workshop (ICCW)*, Jun. 2015.
- [14] W. b. Abbas, F. Gomez-Cuba, and M. Zorzi, "mmWave receiver beamforming comparison tool." [Online]. Available: <http://enigma.det.uvigo.es/~fgomez/mmWaveADCwebviewer/>
- [15] M. R. Akdeniz *et al.*, "Millimeter wave channel modeling and cellular capacity evaluation," *IEEE Journal on Selected Areas in Communications*, vol. 32, no. 6, pp. 1164–1179, Jun. 2014.
- [16] P. A. Elias, S. Rangan, and T. S. Rappaport, "Low-rank spatial channel estimation for millimeter wave cellular systems," *IEEE Transactions on Wireless Communications*, vol. 16, no. 5, pp. 2748–2759, May 2017.
- [17] J. Mo, P. Schniter, N. G. Prelcic, and R. W. Heath, "Channel estimation in millimeter wave MIMO systems with one-bit quantization," in *2014 48th Asilomar Conference on Signals, Systems and Computers*, Nov. 2014, pp. 957–961.
- [18] S. Jacobsson, G. Durisi, M. Coldrey, U. Gustavsson, and C. Studer, "Throughput analysis of massive MIMO uplink with low-resolution adcs," *IEEE Transactions on Wireless Communications*, vol. 16, no. 6, pp. 4038–4051, June 2017.
- [19] J. A. Nossek and M. T. Ivrlac, "Capacity and coding for quantized MIMO systems." in *Proceedings of the International Conference on Wireless Communications and Mobile Computing, (IWCMC 2006)*, 2006.
- [20] B. M. Murray and I. B. Collings, "AGC and quantization effects in a zero-forcing MIMO wireless system," in *IEEE 63rd Vehicular Technology Conference*, vol. 4, May 2006, pp. 1802–1806.
- [21] A. Mezghani and J. A. Nossek, "Capacity lower bound of MIMO channels with output quantization and correlated noise," in *IEEE International Symposium on Information Theory Proceedings (ISIT)*, 2012.
- [22] J. Singh, O. Dabeer, and U. Madhow, "On the limits of communication with low-precision analog-to-digital conversion at the receiver," *IEEE Transactions on Communications*, vol. 57, no. 12, pp. 3629–3639, Dec. 2009.
- [23] Q. Bai, A. Mezghani, and J. A. Nossek, "On the optimization of ADC resolution in multi-antenna systems," in *Proceedings of the Tenth International Symposium on Wireless Communication Systems (ISWCS 2013)*, Aug. 2013.
- [24] O. Orhan, E. Erkip, and S. Rangan, "Low power analog-to-digital conversion in millimeter wave systems: Impact of resolution and bandwidth on performance," in *Information Theory and Applications Workshop (ITA)*, Feb. 2015.
- [25] J. Mo, A. Alkhateeb, S. Abu-Surra, and R. W. Heath, "Hybrid architectures with few-bit adc receivers: Achievable rates and energy-rate tradeoffs," *IEEE Transactions on Wireless Communications*, vol. 16, no. 4, pp. 2274–2287, Apr. 2017.
- [26] X. Gao *et al.*, "Energy-efficient hybrid analog and digital precoding for mmwave MIMO systems with large antenna arrays," *IEEE Journal on Selected Areas in Communications*, vol. 34, no. 4, pp. 998–1009, Apr. 2016.

- [27] R. Mendez-Rial, C. Rusu, N. Gonzalez-Prelcic, A. Alkhateeb, and R. Heath, "Hybrid MIMO architectures for millimeter wave communications: Phase shifters or switches?" *IEEE Access*, vol. 4, pp. 247–267, Jan. 2016.
- [28] L. Fan, S. Jin, C.-K. Wen, and H. Zhang, "Uplink achievable rate for massive MIMO systems with low-resolution ADC," *IEEE Communications Letters*, vol. 19, no. 12, pp. 2186–2189, Dec. 2015.
- [29] J. Zhang, L. Dai, S. Sun, and Z. Wang, "On the spectral efficiency of massive MIMO systems with low-resolution ADCs," *IEEE Communications Letters*, vol. 20, no. 5, pp. 842–845, May 2016.
- [30] A. Alkhateeb, O. El Ayach, G. Leus, and R. Heath, "Channel estimation and hybrid precoding for millimeter wave cellular systems," *IEEE Journal of Selected Topics in Signal Processing*, vol. 8, no. 5, pp. 831–846, Oct. 2014.
- [31] T. Rappaport, R. Heath, R. Daniels, and J. Murdock, *Millimeter Wave Wireless Communications*, ser. Prentice Hall Communications Engineering and Emerging Technologies Series. Pearson Education, 2014.
- [32] C. Mollén, J. Choi, E. G. Larsson, and R. W. Heath, "Uplink performance of wideband massive MIMO with one-bit adcs," *IEEE Transactions on Wireless Communications*, vol. 16, no. 1, pp. 87–100, 2017.
- [33] A. K. Fletcher, S. Rangan, V. K. Goyal, and K. Ramchandran, "Robust predictive quantization: Analysis and design via convex optimization," *IEEE Journal of Selected Topics in Signal Processing*, vol. 1, no. 4, pp. 618–632, Dec 2007.
- [34] C. Barati, S. Hosseini, S. Rangan, P. Liu, T. Korakis, S. Panwar, and T. Rappaport, "Directional cell discovery in millimeter wave cellular networks," *IEEE Transactions on Wireless Communications*, vol. 14, no. 12, pp. 6664–6678, Dec. 2015.
- [35] J. A. Tropp, I. S. Dhillon, R. W. Heath, and T. Strohmer, "Designing structured tight frames via an alternating projection method," *IEEE Trans. Inf. Theor.*, vol. 51, no. 1, pp. 188–209, Jan. 2005.
- [36] Y. Yu *et al.*, "A 60 GHz phase shifter integrated with LNA and PA in 65 nm CMOS for phased array systems," *IEEE Journal of Solid-State Circuits*, vol. 45, no. 9, pp. 1697–1709, Sep. 2010.
- [37] L. Kong, "Energy-efficient 60 GHz phased-array design for multi-Gb/s communication systems," *Ph.D. dissertation, EECS Department, University of California, Berkeley*, Dec. 2014. [Online]. Available: <http://digitalassets.lib.berkeley.edu/techreports/ucb/text/EECS-2014-191.pdf>
- [38] Y.-H. Lin and H. Wang, "A low phase and gain error passive phase shifter in 90 nm CMOS for 60 GHz phase array system application," in *2016 IEEE MTT-S International Microwave Symposium (IMS)*, May 2016, pp. 1–4.
- [39] M. Kraemer *et al.*, "Design of a very low-power, low-cost 60 GHz receiver front-end implemented in 65 nm CMOS technology," *International Journal of Microwave and Wireless Technologies*, vol. 3, pp. 131–138, Apr. 2011.
- [40] H.-S. Lee and C. Sodini, "Analog-to-digital converters: Digitizing the analog world," *Proceedings of the IEEE*, vol. 96, no. 2, pp. 323–334, Feb. 2008.
- [41] R. Mendez-Rial, C. Rusu, A. Alkhateeb, N. Gonzalez-Prelcic, and R. Heath, "Channel estimation and hybrid combining for mmwave: Phase shifters or switches?" in *Information Theory and Applications Workshop (ITA)*, Feb. 2015.
- [42] B. Murmann, "ADC performance survey 1997-2016." [Online]. Available: <http://web.stanford.edu/~murmann/adcsurvey.html>
- [43] B. Nasri, S. P. Sebastian, K.-D. You, R. RanjithKumar, and D. Shahrjerdi, "A 700W 1 GS/s 4-bit folding-flash ADC in 65nm CMOS for wideband wireless communications." [Online]. Available: <https://arxiv.org/abs/1612.04855>